Quantum Aspects of Stimulated Hawking Radiation in an Optical Analog White-Black Hole Pair

Ivan Agullo,* Anthony J. Brady,† and Dimitrios Kranas‡
Department of Physics and Astronomy, Louisiana State University, Baton Rouge, Louisiana 70803, USA

(Received 27 July 2021; accepted 4 February 2022; published 28 February 2022)

This Letter introduces a synergistic combination of analytical and numerical methods to study the Hawking effect in optical systems containing the analog of a white-black hole pair. Our analytical treatment, based on techniques from Gaussian quantum information, provides a simple and efficient model to describe all aspects of the out-state, including the entanglement between any bipartition. We complement the study with a numerical analysis and apply our tools to investigate the influence that ambient thermal noise and detector inefficiencies have on the out-state. We find that aspects of the Hawking effect that are of quantum origin, i.e., quantum entanglement, are extremely fragile to the influence of inefficiencies and noise. We propose a protocol to amplify and observe these quantum aspects, based on seeding the process with a single-mode squeezed input, opening the door to new possibilities for experimental verification of the Hawking effect.

DOI: 10.1103/PhysRevLett.128.091301

Introduction.—The Hawking effect of spontaneous particle pair creation by black holes [1,2] can be understood as a process of two-mode quantum squeezing triggered by a causal horizon. What makes the phenomenon remarkable is not only the squeezing—which generically appears in other time-dependent spacetimes—but its intrinsic thermal (Planckian) character allowing one to associate a temperature with the horizon. This connection with thermodynamics [3,4] led to a profound and fertile crossroad between diverse areas of physics. There is, therefore, a strong motivation to experimentally confirm this prediction, as well as to explore open issues in Hawking's derivation, such as the role of arbitrarily high energy modes [5] or a potential loss of unitarity [6]. This interest has motivated a plethora of analog models, in which the physics of squeezing generated by causal barriers can be recreated in the laboratory [7–13].

A major challenge for observing aspects of the spontaneous Hawking process, even in analog models, is the extraordinarily weak character of the output, easily masked by ambient noise. A promising alternative is to enhance the intensity of the output by replacing the initial vacuum state with a nonvacuum input, i.e., to focus on the *stimulated* Hawking process. However, although stimulated Hawking radiation has been accessed in laboratory experiments [8,9,12], one can explain the observations made so far as a process of classical amplification of waves. Consequently, the stimulated process has been regarded as containing little value to assert the quantum nature of the Hawking effect [8,12].

The goal of this Letter is to introduce a strategy to enhance the *quantum* aspects of the Hawking process. We point out that stimulating the Hawking effect can also amplify the entanglement between the outputs—not merely their intensities—as long as one chooses appropriate quantum initial states and systematic inefficiencies are sufficiently under control. We describe a protocol to observe the amplified entanglement and to unambiguously identify the main characteristics of the Hawking process and its quantum origin out of observations.

Although the core of our ideas is general, we formulate them in the context of optical systems. The advantage is the possibilities optical systems offer to generate, manipulate, and observe quantum states as well as their entanglement structure [14]. We use units in which $c = \hbar = k_B = 1$.

Setup.—Optical systems provide a popular scenario to recreate the physics of the Hawking process [7,12,15–26]. An electromagnetic pulse propagating in a dielectric medium can locally change the optical properties of the medium, modifying the refractive index (Kerr effect). In this way, by introducing strong pulses in nonlinear materials, one can modify the speed of propagation of weak probes propagating thereon. Probes that are initially faster than the pulse will slow down when trying to overtake it, and if the pulse is strong enough, its rear end will act as an impenetrable (moving) barrier. This is the optical analog of the horizon of a white hole—a region where no signal can enter. Similarly, an analog black hole horizon appears in the front end of the pulse. Since the pair white-black hole propagates with the strong pulse, from now on we will work in the frame comoving with it.

The presence of white-black horizons can also be understood by looking at the dispersion relation for weak probes of frequency ω. A detailed analysis of the dispersion relation of dielectric materials with a subluminal dispersion relation and characterized effectively by a single Sellmeier

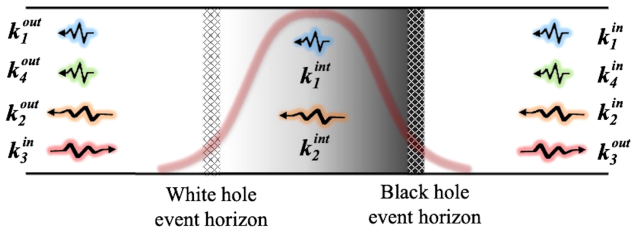

FIG. 1. Illustration of the structure of in, int, and out modes for an optical analog white-black hole in the comoving frame.

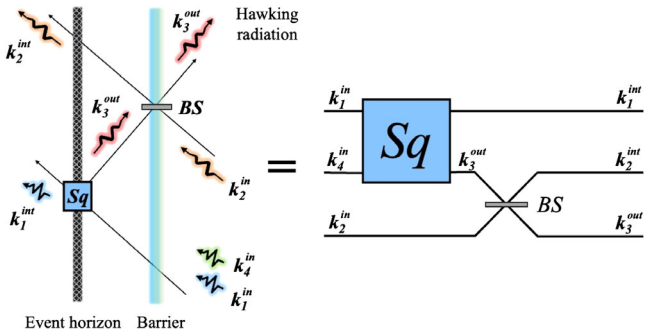

FIG. 2. Left: illustration of the two elements responsible for the Hawking process in optical black holes: a two-mode squeezer associated with the horizon and a beam splitter associated with a process of scattering. Right: equivalent quantum circuit.

term, such as diamond, can be found in [20]. The most relevant features are the following. Far away from the strong pulse, the dispersion relation has four solutions, k_i, $i = 1, \ldots, 4$. The modes k_1 and k_4 are short-wavelength modes, in contrast to k_2 and k_3. The mode k_1 is the only one with negative symplectic norm. Furthermore, k_1, k_2, and k_4 are left movers (negative group velocity), while k_3 wave packets propagate to the right (see Fig. 1). The strong pulse modifies the dispersion relation in such a way that, inside the pulse, the wave numbers k_3 and k_4 become complex and no longer describe propagating modes. Only k_1 and k_2 propagate in the interior region, and since both are left movers, they will necessarily exit the rear end of the pulse. Hence, the interior of the strong pulse is analogous to the interior region of a white-black hole pair.

The analog quantum circuit.—Although the existence of optical horizons originates in nonlinear optics, it is well known that the evolution of weak probes is well approximated by linear equations, and the nonlinearities induced by the strong pulse can be all encoded in the optical properties of the medium. This is the analog of the quantum field theory in curved spacetimes used in Hawking's original derivation. In the optical setup, the resolution of the evolution reduces to computing the scattering matrix (S matrix) describing the dynamics of wave packet modes which, in the asymptotic region, have the wave number centered around k_i^{in}. Since different frequencies ω do not mix with each other—because the properties of the dielectric are time independent in the comoving frame—one computes the S matrix for each individual frequency. We propose an analytical approximation for the S matrix, obtained by combining elementary operations consisting of two-mode squeezers and beam splitters, which we choose by paying attention to the physics of the problem.

For pedagogical purposes, we begin by writing an analog quantum circuit exclusively for the black hole side of the pulse, momentarily neglecting the white hole. In the astrophysical case, the evolution is dominated by two physical processes, a mixing of positive- and negative-frequency modes induced by the horizon, and a scattering process due to the gravitational potential barrier. Mathematically, the first process corresponds to a two-mode squeezer, while the second corresponds to a beam splitter. The situation is analog for optical black holes, except that we have three in modes k_1^{in}, k_2^{in}, and k_4^{in} and three out modes k_1^{int}, k_2^{int}, and k_3^{out} (see Fig. 2).

It is straightforward to convert this circuit into an analytic expression for the S matrix (see Supplemental Material [27]). First, recall the action of a two-mode squeezer on the annihilation operators,

$$\begin{aligned} a_{k_1^{\mathsf{in}}} &\to a_{k_1^{\mathsf{in}}} \cosh r_H + a^\dagger_{k_4^{\mathsf{in}}} e^{i\phi} \sinh r_H, \\ a_{k_4^{\mathsf{in}}} &\to a_{k_4^{\mathsf{in}}} \cosh r_H + a^\dagger_{k_1^{\mathsf{in}}} e^{i\phi} \sinh r_H, \end{aligned} \tag{1}$$

where r_H and ϕ are the intensity and angle, respectively, of the "Hawking squeezer." The action of the beam splitter is the orthogonal transformation

$$\begin{aligned} a_{k_2^{\mathsf{in}}} &\to a_{k_2^{\mathsf{in}}} \cos\theta + a_{k_3^{\mathsf{out}}} \sin\theta, \\ a_{k_3^{\mathsf{out}}} &\to -a_{k_2^{\mathsf{in}}} \sin\theta + a_{k_3^{\mathsf{out}}} \cos\theta, \end{aligned} \tag{2}$$

where $\cos\theta$ and $\sin\theta$ are the transmission and reflection amplitudes of the splitter, respectively. Combining these two operations—following the order written in the circuit—and changing variables to the quadrature operators, $x_i \equiv (1/\sqrt{2})(a_{k_i} + a^\dagger_{k_i})$ and $p_i \equiv [(-i)/\sqrt{2}](a_{k_i} - a^\dagger_{k_i})$, we construct the S matrix corresponding to the circuit in Fig. 2, which, when acting on the vector of quadrature operators $\vec{r}_{\mathsf{in}} = (x_1, p_1, x_2, p_2, x_4, p_4)$, implements the Heisenberg evolution: $\vec{r}_{\mathsf{out}} = S \cdot \vec{r}_{\mathsf{in}}$.

With this formalism, it is particularly easy to evolve any Gaussian state, such as the vacuum, coherent, squeezed, or thermal states. Note that a Gaussian state is completely characterized by its first and second moments, $\vec{\mu} \equiv \langle \vec{r} \rangle$ and $\sigma \equiv \langle \{(\vec{r} - \vec{\mu}), (\vec{r} - \vec{\mu})^\top\} \rangle$, where σ is the covariance matrix and $\{\cdot, \cdot\}$ is the anticommutator (see, e.g., [28,29]). Because linear evolution preserves Gaussianity, given an initial Gaussian state $(\vec{\mu}_{\mathsf{in}}, \sigma_{\mathsf{in}})$, the final state is also Gaussian, characterized by $(\vec{\mu}_{\mathsf{out}}, \sigma_{\mathsf{out}}) = (S \cdot \vec{\mu}_{\mathsf{in}}, S \cdot \sigma_{\mathsf{in}} \cdot S^\top)$.

Regarding the white hole, since it is the time reversal of the black hole, its analog quantum circuit and corresponding

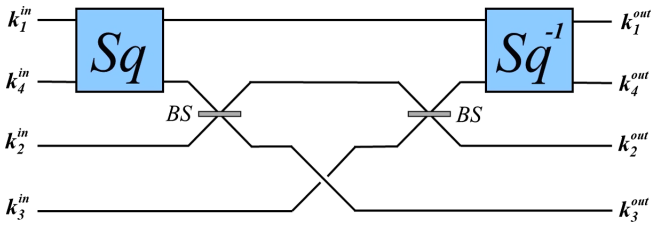

FIG. 3. White-black hole analog quantum circuit.

S matrix can be easily obtained by inverting the elements in the black hole circuit. Combining the two, one obtains the analog circuit for the complete white-black hole system (see Fig. 3). The S matrix for the white-black hole system is then obtained by multiplying the action of squeezers and beam splitters in the sequence indicated in the circuit. The result is an 8×8 matrix that depends on three parameters: r_H, θ, and the phase ϕ.

Numerical analysis.—In order to test the accuracy at which our analog circuit describes the physics of the white-black hole system, we have solved the dynamical evolution numerically (see [16,17,30–39] for previous numerical efforts). We summarize here the most important results of our analysis (a detailed description will appear in [40]).

Our code is based on the analytical model proposed in [20], building on previous work [41] and rooted in the Hopfield model [42]. We solve the dynamical equation in the frequency domain, which is a fourth-order ordinary differential equation in the comoving frame [Eq. (11) in [20]]. We compute the evolution of in wave packets $u^{\mathsf{in}}_{k_i}(t_{\mathsf{in}})$, with wave numbers centered on each of the four solutions of the dispersion relation $(k_1^{\mathsf{in}}, k_2^{\mathsf{in}}, k_3^{\mathsf{in}}, k_4^{\mathsf{in}})$ and with initial spatial support far away from the white-black hole. After evolving each wave packet, we decompose the result in the basis of out wave packets centered around $(k_1^{\mathsf{out}}, k_2^{\mathsf{out}}, k_3^{\mathsf{out}}, k_4^{\mathsf{out}})$, $u^{\mathsf{in}}_{k_i}(t_{\mathsf{out}}) = \sum_j \alpha_{ij} u^{\mathsf{out}}_{k_j}(t_{\mathsf{out}}) + \beta_{ij} \bar{u}^{\mathsf{out}}_{k_j}(t_{\mathsf{out}})$, where the bar denotes complex conjugation. The Bogoliubov coefficients α_{ij} and β_{ij} encode the dynamics, and from them we construct the S matrix.

We model the perturbation of the refractive index as $\delta n(x,t) = \delta n_0 \mathrm{sech}^2[(t - x/u)/\Delta]$ (a common choice in the literature [7,12]), where u is the speed of the perturbation, x and t are spacetime coordinates in the lab frame, and δn_0 and Δ determine its amplitude and width, respectively. We have performed simulations for δn_0 and Δ ranging from 0.01 to 0.1 and from 2 to 10 fs, respectively. We find this is the range for which the analogy with the Hawking effect works better (see below).

For $\Delta \gtrsim 4$ fs and $0.1 \leq \omega/T_H \leq 5$, the circuit in Fig. 3 provides a good approximation for the dynamics, with agreement at the level of (or better than) a percent. In this regime, we confirm that the intensity of the Hawking squeezer r_H, when computed for different frequencies, follows a Planckian distribution, in the sense that $\coth^2 r_H \approx \exp\{\omega/T_H\}$ with a temperature T_H, which agrees with the analog surface gravity of the horizon at the level of a few percent (see Fig. 4). (Deviations at the percent level are expected due to dispersive effects.) For instance, we find $T_H = 10.4$ K for $(\Delta = 4$ fs, $\delta n_0 = 0.1)$, $T_H = 3.51$ K for $(\Delta = 6$ fs, $\delta n_0 = 0.05)$, and $T_H = 0.52$ K for $(\Delta = 8$ fs, $\delta n_0 = 0.01)$ for diamond, for which the refractive index is approximately given by $n^2(\lambda) = 1 + [4.658\lambda^2/(\lambda^2 - 112.5^2)]$ [43], where λ is the free-space wavelength measured in the lab frame and expressed in nanometers.

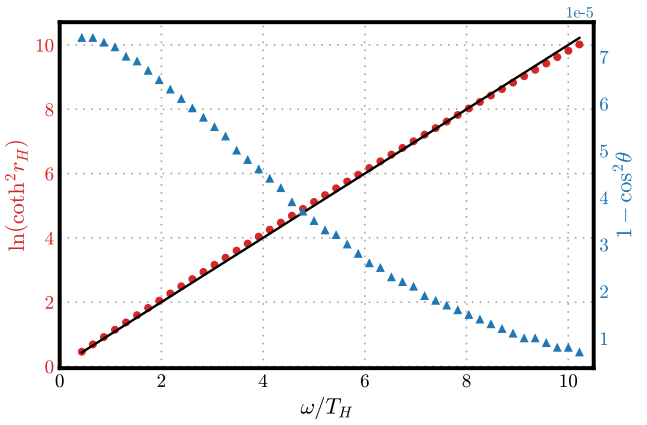

FIG. 4. Left axis (red dots): numerical results for $\ln(\coth^2 r_H)$ vs ω for a strong pulse determined by $\Delta = 6$ fs and $\delta n = 0.05$. We also show the straight line fit ω/T_H, with $T_H = 3.51$ K. Right axis (blue triangles): deviation of the beam splitter transmission probability from unity $(1 - \cos^2\theta)$ vs ω.

The analysis also reveals interesting subtleties: (i) If the pulse width Δ and/or the intensity δn_0 are very small, the tunneling probability for the in mode k_3^{in} to cross the white hole and exit on the black hole side as k_3^{out} becomes non-negligible. This effect is more pronounced for low frequencies. For instance, for $\Delta = 2$ fs and $\delta n_0 = 0.01$, this effect introduces order-one discrepancies between the numerics and our analytical circuit for $\omega/T_H \lesssim 0.1$, although the discrepancies quickly decrease for larger ω or larger values of Δ and/or δn_0. This is an intrinsic limitation of optical analog models, rooted in the fact that right moving modes in the region between the two horizons do actually exist—in contrast to the astrophysical case—although they have exponentially decaying amplitudes. See [44] for a previous analysis on this tunneling effect. (ii) We observe a mixing between k_2^{in} and k_1^{out} slightly higher than predicted by our circuit. Since these modes have symplectic norms of different signs, this implies that there is another contribution to particle creation, originating from scattering and unrelated to the Hawking process. Such contribution was discussed in a different context in [45]. We find that this additional particle creation is nonthermal. It impacts the mean number of output quanta in the mode k_2^{out} and its relevance is more important for large frequencies. However, the impact on the most relevant output channels

for the Hawking effect—the modes k_1^{out}, k_3^{out}, and k_4^{out}—is negligible for $\omega/T_H \lesssim 5$ in all our simulations.

Stimulated Hawking process.—We have explored the evolution of a family of Gaussian initial states and have studied the output intensities and entanglement structure generated during the Hawking process. We quantify the entanglement by means of the logarithmic negativity (LN) [46,47] (for previous discussion of entanglement in other analog models, see [24,33,48–58]). LN is based on the Peres-Horodecki criterion [59,60], similar to other inequalities used in some previous works (see, e.g., [52]). But LN has the additional advantage that it is an entanglement *quantifier*; i.e., it can be used to quantify the amount of entanglement and not only to signal its presence. This is important for our goals. An interesting observation is that nonclassical inputs (squeezed states) alter the covariance of the final state and can be used to amplify the entanglement generated by the Hawking process. This is not possible with coherent state inputs, since they have the same covariance matrix as the vacuum. Using our formalism, we can obtain analytical expressions for the main aspects of the out-state (given any initial state) in terms of the open parameters r_H, θ, and ϕ of the circuit, the latter of which we determine numerically and are obviously independent of the quantum states chosen for the weak probes.

We have incorporated the effect of losses (e.g., detector inefficiencies) and ambient noise, both ubiquitous in real experiments. Noise (e.g., a thermal environment) can be incorporated by adding n_{env} photons to each input mode, while the effects of inefficiencies can be modeled by the following transformation of the final state: $\vec{\mu}_{\text{out}} \to \sqrt{\eta}\vec{\mu}_{\text{out}}$, $\sigma_{\text{out}} \to \eta\sigma_{\text{out}} + (1-\eta)\mathbb{I}$, where $0 \le \eta \le 1$ is the attenuation factor. In the calculations below, we add the same amount of noise and inefficiencies to all channels, although this can be generalized straightforwardly.

A simple protocol.—We find that a convenient strategy is to illuminate the white hole with a single-mode squeezed state in the long-wavelength mode k_3^{in} and observe the Hawking pair of modes $(k_1^{\text{out}}, k_4^{\text{out}})$ leaving the white hole (see Fig. 1). This strategy produces an optimal amount of entanglement enhancement, carried by the $(k_1^{\text{out}}, k_4^{\text{out}})$ mode pair, and more importantly, it allows us to recover the information about the Hawking process in a simple manner, as we now describe.

From the quantum circuit, we find that the mean particle number $\langle n_{k_i}^{\text{out}} \rangle$ for $i = 1, 4$ grows *linearly* with $\sinh^2 r_{k_3}^{\text{in}}$, where $r_{k_3}^{\text{in}}$ is the squeezing intensity chosen for the input state. The rates of these linear growths are

$$m_{k_1^{\text{out}}} = \eta(1 + 2n_{\text{env}})\cos^2\theta \sinh^2 r_H,$$
$$m_{k_4^{\text{out}}} = \eta(1 + 2n_{\text{env}})\cos^2\theta \cosh^2 r_H. \tag{3}$$

These rates can be determined in the lab by measuring the intensity of the output modes while tuning the initial squeezing $r_{k_3}^{\text{in}}$. By taking ratios, one can obtain the intensity of the Hawking squeezer $r_H(\omega)$ as $m_{k_4^{\text{out}}}/m_{k_1^{\text{out}}} = \coth^2 r_H$. The effects of thermal noise and inefficiencies cancel out in this ratio.

Although this protocol permits one to reconstruct the properties of the Hawking squeezer $r_H(\omega)$, it is based on intensities and does not involve any genuinely quantum property. Interestingly, the $r_H(\omega)$ can be independently reconstructed from the entanglement (LN) between the Hawking pair $(k_1^{\text{out}}, k_4^{\text{out}})$ emitted by the white hole. The analytical expression for the LN between these two modes is lengthy, and its behavior with the initial squeezing intensity $r_{k_3}^{\text{in}}$ is better illustrated in Fig. 5. There are two important takeaway messages from our analysis: (i) In the absence of the Hawking squeezer, $r_H(\omega) = 0$, there is no entanglement between k_1^{out}, k_4^{out} (not explicitly shown in Fig. 5), no matter what the value of the initial single-mode squeezing $r_{k_3}^{\text{in}}$ is. Therefore, the observation of such entanglement must be attributed to the Hawking effect, and not to the initial state, which contains no entanglement between these two modes. (ii) The LN increases monotonically with the initial squeezing intensity $r_{k_3}^{\text{in}}$ (if inefficiencies are small; see below), and thus initial squeezing enhances the quantum properties of the output. Obtaining the LN, for instance, by reduced-state reconstruction using homodyne measurements [14], and comparing with the theoretical curves in Fig. 5, the Hawking squeezing strength $r_H(\omega)$ can be obtained from a quantity of purely quantum origin. The value of $r_H(\omega)$ obtained in this way

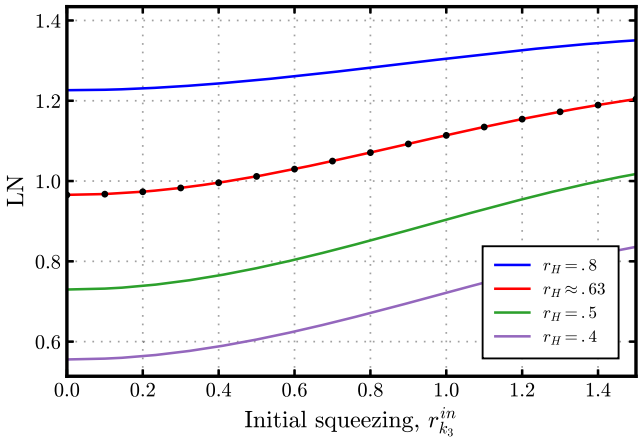

FIG. 5. Stimulating the white hole for entanglement enhancement. Continuous lines: LN between the outgoing white-hole partner modes k_1^{out} and k_4^{out} vs the initial squeezing intensity $r_{k_3}^{\text{in}}$, computed from the circuit model for various values of the Hawking squeezing strength r_H. Curves from top to bottom indicate decreasing values of r_H. Dots: results from the numerical simulations evaluated at $\omega/T_H = 1.08$ (same conditions as Fig. 4). Noise parameters are $n_{\text{env}} = (e^{w/(T_H/2)} - 1)^{-1}$ and $\eta = 0.9$.

must agree with the one independently obtained from intensities [Eqs. (3)], providing a strong consistency test.

To illustrate the way this protocol works, we have added to Fig. 5 the results for the LN obtained from numerical simulation, for different initial squeezing $r_{k_3}^{\mathrm{in}}$. The numerical simulations are completely independent from our analytical calculations. By comparing with a family of theoretical curves obtained for different r_H, we can identify the value of the Hawking squeezing intensity $r_H(\omega)$ that corresponds to the numerical simulations. In a real experiment, one would proceed in a similar fashion, by replacing the numerically generated points in Fig. 5 with experimental data. One needs to make sure that the initial squeezing is not too large to trigger substantial nonlinear effects, such as those discussed in [61].

We now discuss the effects of noise and inefficiencies. Noise systematically reduces the entanglement in the final state, even causing it to vanish if the environment number of photons n_{env} is large enough. For instance, for vacuum input, the entanglement in the bipartition $(k_1^{\mathrm{out}}|k_4^{\mathrm{out}})$ disappears when n_{env} is larger than a frequency-dependent threshold, which we find to be equal to $(e^{\omega/T_H}-1)^{-1}$ for low frequencies ($\omega/T_H \ll 1$) and equal to $e^{-\omega/(2T_H)}$ for large frequencies ($\omega/T_H \gg 1$). This last result is in agreement with previous findings in [50]. In the absence of inefficiencies ($\eta \approx 1$), squeezing a single mode in the initial state can *always* be used to overcome these thresholds and restore the entanglement.

On the other hand, entanglement is sensitive to the effects of inefficiencies even when initial squeezing is present. In particular, for values of the attenuation parameter η smaller than a critical value η_c, the effect of squeezing the input is reversed, and initial squeezing *degrades* the entanglement in the output. For instance, we find $\eta_c \approx 0.8$ for $\omega/T_H = 1$, while $\eta_c \approx 0.9$ for $\omega/T_H = 4$.

Conclusions.—Our analytical treatment presents two main advantages: (i) its generality—it is not based on any concrete model of the optical media, and in fact, it can be applied to other, nonoptical analog models (see [58], where related techniques have been recently discussed in Bose-Einstein condensates); (ii) its capabilities—it allows us to compute in a few lines all aspects of the output channels, including the entire entanglement structure. We have complemented the model with a numerical simulation, which we use to check its validity, determine its free parameters, and delimit its regime of applicability. We have analyzed the effects of background noise and inefficiencies and found that quantum entanglement is easily masked, or completely erased, by these deleterious effects.

Furthermore, we have introduced a strategy to amplify the quantum features and overcome entanglement-degrading effects and have proposed a protocol to observe them in the lab. Although additional difficulties may arise in a real experiment, our ideas constitute a step forward in the observability of the Hawking process.

We have benefited from discussions with A. Fabbri, J. Pullin, J. Olmedo, and especially with O. Magana-Loaiza. We thank J. Olmedo for assistance with Fig. 4. This work is supported by the NSF Grants No. CAREER PHY-1552603 and No. PHY-2110273 and from the Hearne Institute for Theoretical Physics.

*agullo@lsu.edu
†abrady6@lsu.edu
‡dkrana1@lsu.edu

[1] S. W. Hawking, Black hole explosions, Nature (London) **248**, 30 (1974).
[2] S. W. Hawking, Particle creation by black holes, Commun. Math. Phys. **43**, 199 (1975); **46**, 206(E) (1976).
[3] J. M. Bardeen, B. Carter, and S. W. Hawking, The four laws of black hole mechanics, Commun. Math. Phys. **31**, 161 (1973).
[4] J. D. Bekenstein, Generalized second law of thermodynamics in black hole physics, Phys. Rev. D **9**, 3292 (1974).
[5] T. Jacobson, Black hole evaporation and ultrashort distances, Phys. Rev. D **44**, 1731 (1991).
[6] S. W. Hawking, Breakdown of predictability in gravitational collapse, Phys. Rev. D **14**, 2460 (1976).
[7] Thomas G. Philbin, Chris Kuklewicz, Scott Robertson, Stephen Hill, Friedrich König, and Ulf Leonhardt, Fiber-optical analog of the event horizon, Science **319**, 1367 (2008).
[8] Silke Weinfurtner, Edmund W. Tedford, Matthew C. J. Penrice, William G. Unruh, and Gregory A. Lawrence, Measurement of Stimulated Hawking Emission in an Analogue System, Phys. Rev. Lett. **106**, 021302 (2011).
[9] L.-P. Euvé, F. Michel, R. Parentani, T. G. Philbin, and G. Rousseaux, Observation of Noise Correlated by the Hawking Effect in a Water Tank, Phys. Rev. Lett. **117**, 121301 (2016).
[10] Jeff Steinhauer, Observation of quantum Hawking radiation and its entanglement in an analogue black hole, Nat. Phys. **12**, 959 (2016).
[11] Juan Ramon Munoz de Nova, Katrine Golubkov, Victor I. Kolobov, and Jeff Steinhauer, Observation of thermal Hawking radiation and its temperature in an analogue black hole, Nature (London) **569**, 688 (2019).
[12] Jonathan Drori, Yuval Rosenberg, David Bermudez, Yaron Silberberg, and Ulf Leonhardt, Observation of Stimulated Hawking Radiation in an Optical Analogue, Phys. Rev. Lett. **122**, 010404 (2019).
[13] Victor I. Kolobov, Katrine Golubkov, Juan Ramón Muñoz de Nova, and Jeff Steinhauer, Observation of stationary spontaneous Hawking radiation and the time evolution of an analogue black hole, Nat. Phys. **17**, 362 (2021).
[14] A. I. Lvovsky and M. G. Raymer, Continuous-variable optical quantum-state tomography, Rev. Mod. Phys. **81**, 299 (2009).
[15] A. Demircan, Sh Amiranashvili, and G. Steinmeyer, Controlling Light by Light with an Optical Event Horizon, Phys. Rev. Lett. **106**, 163901 (2011).
[16] E. Rubino, A. Lotti, F. Belgiorno, S. L. Cacciatori, A. Couairon, U. Leonhardt, and D. Faccio, Soliton-induced

relativistic-scattering and amplification, Sci. Rep. **2**, 932 (2012).
[17] Mike Petev, Niclas Westerberg, Daniel Moss, Elenora Rubino, C. Rimoldi, S. L. Cacciatori, F. Belgiorno, and D. Faccio, Blackbody Emission from Light Interacting with an Effective Moving Dispersive Medium, Phys. Rev. Lett. **111**, 043902 (2013).
[18] S. Finazzi and I. Carusotto, Quantum vacuum emission in a nonlinear optical medium illuminated by a strong laser pulse, Phys. Rev. A **87**, 023803 (2013).
[19] F. Belgiorno, S. L. Cacciatori, and F. Dalla Piazza, Hawking effect in dielectric media and the Hopfield model, Phys. Rev. D **91**, 124063 (2015).
[20] Malte F. Linder, Ralf Schützhold, and William G. Unruh, Derivation of Hawking radiation in dispersive dielectric media, Phys. Rev. D **93**, 104010 (2016).
[21] D. Bermudez and U. Leonhardt, Hawking spectrum for a fiber-optical analog of the event horizon, Phys. Rev. A **93**, 053820 (2016).
[22] F. Belgiorno, S. L. Cacciatori, F. Dalla Piazza, and M. Doronzo, Hopfield-Kerr model and analogue black hole radiation in dielectrics, Phys. Rev. D **96**, 096024 (2017).
[23] M. J. Jacquet and F. König, Analytical description of quantum emission in optical analogs to gravity, Phys. Rev. A **102**, 013725 (2020).
[24] M. Jacquet and F. Koenig, The influence of spacetime curvature on quantum emission in optical analogues to gravity, SciPost Phys. Core **3**, 005 (2020).
[25] Rosenberg, Yuval, Optical analogues of black-hole horizons, Phil. Trans. R. Soc. A **378**, 20190232 (2020).
[26] R. Aguero-Santacruz and D. Bermudez, Hawking radiation in optics and beyond, Phil. Trans. R. Soc. A **378**, 20190223 (2020).
[27] See Supplemental Material at http://link.aps.org/supplemental/10.1103/PhysRevLett.128.091301 for elements of quantum Gaussian states for bosonic systems and their application to optical horizons.
[28] G. Adesso, S. Ragy, and A. R. Lee, Continuous variable quantum information: Gaussian states and beyond, Open Syst. Inf. Dyn. **21**, 1440001 (2014).
[29] A. Serafini, *Quantum Continuous Variables: A Primer of Theoretical Methods* (CRC Press, Boca Raton, FL, 2017).
[30] J. L. Gaona-Reyes and D. Bermudez, The theory of optical black hole lasers, Ann. Phys. (Amsterdam) **380**, 41 (2017).
[31] A. Moreno-Ruiz and D. Bermudez, Hawking temperature in dispersive media: Analytics and numerics, Ann. Phys. (Amsterdam) **420**, 168268 (2020).
[32] J. Macher and R. Parentani, Black/white hole radiation from dispersive theories, Phys. Rev. D **79**, 124008 (2009).
[33] X. Busch, I. Carusotto, and R. Parentani, Spectrum and entanglement of phonons in quantum fluids of light, Phys. Rev. A **89**, 043819 (2014),
[34] S. Finazzi and R. Parentani, Spectral properties of acoustic black hole radiation: Broadening the horizon, Phys. Rev. D **83**, 084010 (2011).
[35] S. Finazzi and R. Parentani, On the robustness of acoustic black hole spectra, J. Phys. Conf. Ser. **314**, 012030 (2011).
[36] S. Finazzi and R. Parentani, Hawking radiation in dispersive theories, the two regimes, Phys. Rev. D **85**, 124027 (2012).
[37] F. Michel and R. Parentani, Probing the thermal character of analogue Hawking radiation for shallow water waves?, Phys. Rev. D **90**, 044033 (2014).
[38] F. Michel, J.-F. Coupechoux, and R. Parentani, Phonon spectrum and correlations in a transonic flow of an atomic Bose gas, Phys. Rev. D **94**, 084027 (2016).
[39] S. Robertson, C. Ciret, S. Massar, S.-P. Gorza, and R. Parentani, Four-wave mixing and enhanced analog Hawking effect in a nonlinear optical waveguide, Phys. Rev. A **99**, 043825 (2019).
[40] I. Agullo, A. Brady, and D. Kranas (to be published).
[41] F. Belgiorno, S. L. Cacciatori, and F. Dalla Piazza, Hawking effect in dielectric media and the Hopfield model, Phys. Rev. D **91**, 124063 (2015).
[42] J. Hopfield, Theory of the contribution of excitons to the complex dielectric constant of crystals, Phys. Rev. **112**, 1555 (1958).
[43] G. Turri, S. Webster, Y. Chen, B. Wickham, A. Bennett, and M. Bass, Index of refraction from the near-ultraviolet to the near-infrared from a single crystal microwave-assisted cvd diamond, Opt. Mater. Express **7**, 855 (2017).
[44] A. Choudhary and F. König, Efficient frequency shifting of dispersive waves at solitons, Opt. Express **20**, 5538 (2012).
[45] S. Corley and T. Jacobson, Hawking spectrum and high frequency dispersion, Phys. Rev. D **54**, 1568 (1996).
[46] G. Vidal and R. F. Werner, Computable measure of entanglement, Phys. Rev. A **65**, 032314 (2002).
[47] M. B. Plenio, Logarithmic Negativity: A Full Entanglement Monotone that is not Convex, Phys. Rev. Lett. **95**, 090503 (2005).
[48] B. Horstmann, B. Reznik, S. Fagnocchi, and J. I. Cirac, Hawking Radiation from an Acoustic Black Hole on an Ion Ring, Phys. Rev. Lett. **104**, 250403 (2010).
[49] S. Giovanazzi, Entanglement Entropy and Mutual Information Production Rates in Acoustic Black Holes, Phys. Rev. Lett. **106**, 011302 (2011).
[50] David Edward Bruschi, Nicolai Friis, Ivette Fuentes, and Silke Weinfurtner, On the robustness of entanglement in analogue gravity systems, New J. Phys. **15**, 113016 (2013).
[51] S. Finazzi and I. Carusotto, Entangled phonons in atomic Bose-Einstein condensates, Phys. Rev. A **90**, 033607 (2014).
[52] X. Busch and R. Parentani, Quantum entanglement in analogue Hawking radiation: When is the final state nonseparable?, Phys. Rev. D **89**, 105024 (2014).
[53] D. Boiron, A. Fabbri, P. E. Larré, N. Pavloff, C. I. Westbrook, and P. Zin, Quantum Signature of Analog Hawking Radiation in Momentum Space, Phys. Rev. Lett. **115**, 025301 (2015).
[54] J. R. M. de Nova, F. Sols, and I. Zapata, Entanglement and violation of classical inequalities in the Hawking radiation of flowing atom condensates, New J. Phys. **17**, 105003 (2015).
[55] A. Fabbri and N. Pavloff, Momentum correlations as signature of sonic Hawking radiation in Bose-Einstein condensates, SciPost Phys. **4**, 019 (2018).
[56] A. Coutant and S. Weinfurtner, Low frequency analogue Hawking radiation: The Bogoliubov-de Gennes model, Phys. Rev. D **97**, 025006 (2018).

[57] Y. Nambu and Y. Osawa, Tripartite entanglement of Hawking radiation in dispersive model, Phys. Rev. D **103**, 125007 (2021).

[58] M. Isoard, N. Milazzo, N. Pavloff, and O. Giraud, Bipartite and tripartite entanglement in a Bose-Einstein acoustic black hole, Phys. Rev. A **104**, 063302 (2021).

[59] A. Peres, Separability Criterion for Density Matrices, Phys. Rev. Lett. **77**, 1413 (1996).

[60] M. Horodecki, P. Horodecki, and R. Horodecki, Separability of mixed states: necessary and sufficient conditions, Phys. Lett. A **223**, 1 (1996).

[61] S. Robertson, F. Michel, and R. Parentani, Nonlinearities induced by parametric resonance in effectively 1D atomic Bose condensates, Phys. Rev. D **98**, 056003 (2018).